

Single photo and electroproduction of pions at EBAC@JLAB

B. Julia-Diaz^{1,2)}

1 (Department d'Estructura i Constituents de la Matèria and Institut de Ciències del Cosmos, Universitat de Barcelona, E-08028 Barcelona, Spain)

2 (Excited Baryon Analysis Center (EBAC), Thomas Jefferson National Accelerator Facility, Newport News, VA 23606, USA)

Abstract

Within the Excited Baryon Analysis Center we have performed a dynamical coupled-channels analysis of the available $p(e, e'\pi)N$ data in the region of $W \leq 1.6$ GeV and $Q^2 \leq 1.45$ (GeV/c)². The channels included are γ^*N , πN , ηN , and $\pi\pi N$ which has $\pi\Delta$, ρN , and σN components. With the hadronic parameters of the model determined in our previous investigations of $\pi N \rightarrow \pi N$ reaction, we have found that the available data in the considered $W \leq 1.6$ GeV region can be fitted well by only adjusting the bare $\gamma^*N \rightarrow N^*$ helicity amplitudes for the lowest N^* states in P_{33} , P_{11} , S_{11} and D_{13} partial waves. The meson cloud effect, as required by the unitarity conditions, on the $\gamma^*N \rightarrow N^*$ form factors are examined.

Key words meson electroproduction, helicity amplitudes

PACS 13.75.Gx, 13.60.Le, 14.20.Gk

1 Introduction

The electromagnetic parameters characterizing the excited nucleons, N^* , and in particular the $\gamma^*N \rightarrow N^*$ form factors, are important information for understanding the hadron structure within Quantum Chromodynamics (QCD). Thanks to the efforts in recent years, as reviewed in Ref. [1], the world data of $\gamma^*N \rightarrow \Delta(1232)$ form factors are considered along with the electromagnetic nucleon form factors as the benchmark data for developing hadron structure models and testing predictions from Lattice QCD calculations (LQCD).

In the present work, we explore the extent to which the available $p(e, e'\pi)N$ data in $W \leq 1.6$ GeV can be used to extract the $\gamma^*N \rightarrow N^*$ form factors for the N^* states up to the so-called “second” resonance region.

We employ a dynamical coupled-channels model developed in Refs. [2, 3, 4, 5, 6] and extend our analysis^[4] of pion photoproduction reactions. We therefore will only recall equations which are relevant to the coupled-channels calculations of $p(e, e'\pi)N$ cross sections. In the helicity-LSJ mixed-representation where the initial γN state is specified by its helicities λ_γ and λ_N and the final MB states by the $(LS)J$ angular momentum variables, the reaction amplitude of

$\gamma^*(\vec{q}, Q^2) + N(-\vec{q}) \rightarrow \pi(\vec{k}) + N(-\vec{k})$ at invariant mass W and momentum transfer $Q^2 = -q^\mu q_\mu = \vec{q}^2 - \omega^2$ can be written within a Hamiltonian formulation^[2] as (suppress the isospin quantum numbers)

$$T_{LSN\pi N, \lambda_\gamma \lambda_N}^J(k, q, W, Q^2) = t_{LSN\pi N, \lambda_\gamma \lambda_N}^J(k, q, W, Q^2) + t_{LSN\pi N, \lambda_\gamma \lambda_N}^{R, J}(k, q, W, Q^2) \quad (1)$$

where $S_N = 1/2$ is the nucleon spin, $W = \omega + E_N(q)$ is the invariant mass of the γ^*N system, and the non-resonant amplitude is

$$t_{LSN\pi N, \lambda_\gamma \lambda_N}^J(k, q, W, Q^2) = v_{LSN\pi N, \lambda_\gamma \lambda_N}^J(k, q, Q^2) + \sum_{M'B'} \sum_{L'S'} \int k'^2 dk' t_{LSN\pi N, L'S'M'B'}^J(k, k', W) \times G_{M'B'}(k', W) v_{L'S'M'B', \lambda_\gamma \lambda_N}^J(k', q, Q^2) \quad (2)$$

In the above equation, $G_{M'B'}(k', W)$ are the meson-baryon propagators for the channels $M'B' = \pi N, \eta N, \pi\Delta, \rho N, \sigma N$. The matrix elements $v_{LSMB, \lambda_\gamma \lambda_N}^J(k, q, Q^2)$, which describe the $\gamma N \rightarrow MB$ transitions, are given explicitly in Appendix F of Ref. [2]. The hadronic non-resonant amplitudes $t_{LSN\pi N, L'S'M'B'}^J(k, k', W)$ are generated from the model constructed from analyzing the data of $\pi N \rightarrow \pi N$ reactions^[3].

Received 20 June 2009

©2009 Chinese Physical Society and the Institute of High Energy Physics of the Chinese Academy of Sciences and the Institute of Modern Physics of the Chinese Academy of Sciences and IOP Publishing Ltd

The resonant amplitude in Eq. (1) is

$$t_{LSN\pi N, \lambda_\gamma \lambda_N}^{R,J}(k, q, W, Q^2) = \sum_{N_i^*, N_j^*} [\bar{\Gamma}_{N_i^*, LSN\pi N}^J(k, W)]^* D_{i,j}(W) \bar{\Gamma}_{N_j^*, \lambda_\gamma \lambda_N}^J(q, W, Q^2), \quad (3)$$

where the dressed $N^* \rightarrow \pi N$ vertex $\bar{\Gamma}_{N_i^*, LSN\pi N}^J(k, W)$ and N^* propagator $D_{i,j}(W)$ have been determined and given explicitly in Ref. [4]. The quantity relevant to our later discussions is the dressed $\gamma^* N \rightarrow N^*$ vertex function defined by

$$\begin{aligned} \bar{\Gamma}_{N^*, \lambda_\gamma \lambda_N}^J(q, W, Q^2) &= \Gamma_{N^*, \lambda_\gamma \lambda_N}^J(q, Q^2) \\ &+ \sum_{M'B'} \sum_{L'S'} \int k'^2 dk' \bar{\Gamma}_{N^*, L'S'M'B'}^J(k', W) \\ &\times G_{M'B'}(k', W) v_{L'S'M'B', \lambda_\gamma \lambda_N}^J(k', q, Q^2). \end{aligned} \quad (4)$$

Similar to what was defined in Ref. [7, 8], we call the contribution of the second term of Eq. (4) the *meson cloud effect* to define precisely what will be presented in this paper. We emphasize here that the meson cloud term in Eq. (4) is the necessary consequence of the unitarity conditions. How this term and the assumed bare N^* states are interpreted is obviously model dependent.

Within the one-photon exchange approximation, the differential cross sections of pion electroproduction can be written as

$$\begin{aligned} \frac{d\sigma^5}{dE_e' d\Omega_{e'} d\Omega_\pi^*} &= \Gamma_\gamma \left[\sigma_T + \epsilon \sigma_L + \sqrt{2\epsilon(1+\epsilon)} \sigma_{LT} \cos \phi_\pi^* \right. \\ &\quad \left. + \epsilon \sigma_{TT} \cos 2\phi_\pi^* + h_e \sqrt{2\epsilon(1-\epsilon)} \sigma_{LT'} \sin \phi_\pi^* \right]. \end{aligned} \quad (5)$$

Here $\Gamma_\gamma = [\alpha/(2\pi^2 Q^2)](E_e'/E_e)[|\vec{q}_L|/(1-\epsilon)]$; ϵ is defined by the electron scattering angle θ_e and the

photon 3-momentum \vec{q}_L in the laboratory frame as $\epsilon = [1 + 2(|\vec{q}_L|^2/Q^2) \tan^2(\theta_e/2)]^{-1}$; h_e is the helicity of the incoming electron; ϕ_π^* is the angle between the π - N plane and the plane of the incoming and outgoing electrons. The quantities associated with the electrons are defined in the laboratory frame. On the other hand, structure functions of $\gamma^* N \rightarrow \pi N$ process, $\sigma_\alpha = \sigma_\alpha(W, Q^2, \cos \theta_\pi^*)$ ($\alpha = T, L, LT, TT, LT'$), are defined in the final πN center of mass system. The formula for calculating σ_α from the amplitudes defined by Eqs. (1)-(3) are given in Ref. [9].

In this first-stage investigation, we only consider the data of structure functions σ_α of $p(e, e' \pi^0)p$ [10, 11] and $p(e, e' \pi^+)n$ [12, 13] up to $W = 1.6$ GeV and $Q^2 = 1.45$ (GeV/c)². The availability of the data in the corresponding (W, Q^2) region are found in Table 1. The resulting parameters are then confirmed against the original five-fold differential cross section data [14]. This procedure could overestimate/underestimate the errors of our analysis, but is sufficient for the present exploratory investigation.

In section II, we present the results from our analysis. Discussions on future developments are given in section III.

Table 1. Q^2 values, in GeV, for which there are available structure function data ($Q^2 \leq 1.45$ (GeV/c)²). Data from Refs. [10, 11, 12, 13]

	$\sigma_T + \epsilon \sigma_L, \sigma_{LT}, \sigma_{TT}$	$\sigma_{LT'}$
$\gamma^* p \rightarrow \pi^0 p$	0.4, 0.525, 0.65, 0.75, 0.9, 1.15, 1.46	0.4, 0.65
$\gamma^* p \rightarrow \pi^+ n$	0.3, 0.4, 0.5, 0.6	0.4, 0.65

2 Analysis and Results

We parameterize the bare $\gamma^* N \rightarrow N^*$ vertex functions $\Gamma_{N^*, \lambda_\gamma \lambda_N}^J(q, Q^2)$ as

$$\begin{aligned} \Gamma_{N^*, \lambda_\gamma \lambda_N}^J(q, Q^2) &= \frac{1}{(2\pi)^{3/2}} \sqrt{\frac{m_N}{E_N(q)}} \sqrt{\frac{q_R}{|q_0|}} \\ &\times G_\lambda(N^*, Q^2) \delta_{\lambda, (\lambda_\gamma - \lambda_N)}, \end{aligned} \quad (6)$$

where q_R and q_0 are defined by $M_{N^*} = q_R + E_N(q_R)$ with N^* mass and $W = q_0 + E_N(q_0)$, respectively, and

$$\begin{aligned} G_\lambda(N^*, Q^2) &= A_\lambda(N^*, Q^2), \quad \text{transverse photon} \\ &= S_\lambda(N^*, Q^2), \quad \text{longitudinal photon} \end{aligned} \quad (7)$$

For later discussions, we also cast the helicity amplitudes of the dressed vertex Eq. (4) into the form of

Eq. (6) with dressed helicity amplitudes

$$\bar{A}_\lambda(N^*, Q^2) = A_\lambda(N^*, Q^2) + A_\lambda^{\text{m.c.}}(N^*, Q^2), \quad (9)$$

$$\bar{S}_\lambda(N^*, Q^2) = S_\lambda(N^*, Q^2) + S_\lambda^{\text{m.c.}}(N^*, Q^2), \quad (10)$$

where $A_\lambda^{\text{m.c.}}(N^*, Q^2)$ and $S_\lambda^{\text{m.c.}}(N^*, Q^2)$ are due to the meson cloud effect defined by the second term of Eq. (4).

With the hadronic parameters fixed in analyzing the πN reaction data [3, 6], the only freedom in analyzing the electromagnetic meson production reactions are the electromagnetic coupling parameters of the model. If the parameters listed in Ref. [2] are used to calculate the non-resonant interaction $v_{L'S'M'B', \lambda_\gamma \lambda_N}^J(k', q)$ in Eqs. (2) and (4), the only parameters to be determined from the data of pion electroproduction reactions are the bare helicity amplitudes defined by Eq. (6). Such a highly constrained analysis was performed in Ref. [4] for pion photo-

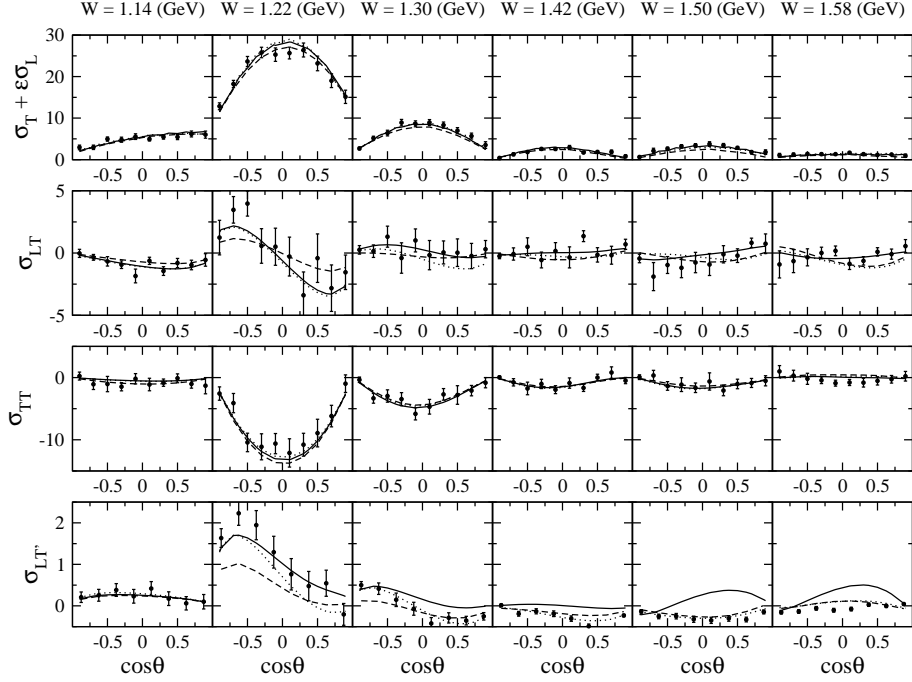


Fig. 1. Fit to $p(e, e' \pi^0)p$ structure functions at $Q^2 = 0.4$ (GeV/c) 2 . Here $\theta \equiv \theta_\pi^*$. The solid curves are the results of Fit1, the dashed curves are of Fit2, and the dotted curves are of Fit3. (See text for the description of each fit.) The data are taken from Refs. [10, 11].

production. It was found that the available data of $\gamma p \rightarrow \pi^0 p$, $\pi^+ n$ can be fitted reasonably well up to invariant mass $W \leq 1.6$ GeV. In this work we extend this effort to analyze the pion electroproduction data in the same W region.

We first try to fix the bare helicity amplitudes by fitting to the data of $\sigma_T + \epsilon\sigma_L$, σ_{LT} , and σ_{TT} of $p(e, e' \pi^0)p$ in Ref. [10] which covers almost all (W, Q^2) region we are considering (see Table. 1). In a purely phenomenological approach, we first vary all of the helicity amplitudes of 16 bare N^* states, considered in analyzing the $\pi N \rightarrow \pi N, \pi\pi N$ data [3, 6], in the fits to the data. It turns out that only the helicity amplitudes of the first N^* states in S_{11} , P_{11} , P_{33} and D_{13} are relevant in the considered $W \leq 1.6$ GeV. Thus only the bare helicity amplitudes associated with those four bare N^* states (total 10 parameters) are varied in the fit and the other bare helicity amplitudes are set to zero. The numerical fit is performed at each Q^2 independently, using the MINUIT library.

The results of our fits are the solid curves in the top three rows of Fig. 1. Clearly our results from this fit agree with the data well. We obtain similar quality of fits to the data of Ref. [10] at other Q^2 values listed in Table. 1. We have also used the magnetic $M1$ form factor of $\gamma^* N \rightarrow \Delta(1232)$ extracted from previous analyses as data for fitting. We refer the results of this fit to as “Fit1”.

The helicity amplitudes of S_{11} , P_{11} , and D_{13} resulting from Fit1 are shown in Fig. 2. The solid circles are the absolute magnitude of the dressed helicity amplitudes (9) and (10). The errors there are assigned by MIGRAD in the MINUIT library. More detailed analysis of the errors is perhaps needed, but will not be addressed here. The meson cloud effect (dashed curves), as defined by $A_\lambda^{\text{m.c.}}$ and $S_\lambda^{\text{m.c.}}$ of Eqs. (9) and (10) and calculated from the second term of Eq. (4), are the necessary consequence of the unitarity conditions. They do not include the bare helicity term determined here and are already fixed in the photoproduction analysis [4]. Within our model (and within Fit1), the meson cloud contribution is relatively small in S_{11} and $A_{1/2}$ of D_{13} even in the low Q^2 region.

Here we note that our helicity amplitudes defined in Eqs. (9) and (10) are different from the commonly used convention, say A_λ^{cnv} and S_λ^{cnv} , which are obtained from the imaginary part of the $\gamma^* N \rightarrow \pi N$ multipole amplitudes [16]. This definition leads to helicity amplitudes which are real, while our dressed amplitudes are complex. It was shown in Ref. [15] that for the $\Delta(1232)$ resonance our dressed helicity amplitudes (9) and (10) can be reduced to A_λ^{cnv} and S_λ^{cnv} , if we replace the Green function $G_{\pi N}$ with its principal value in all loop integrals appearing in the calculation. However, such reduction is not so triv-

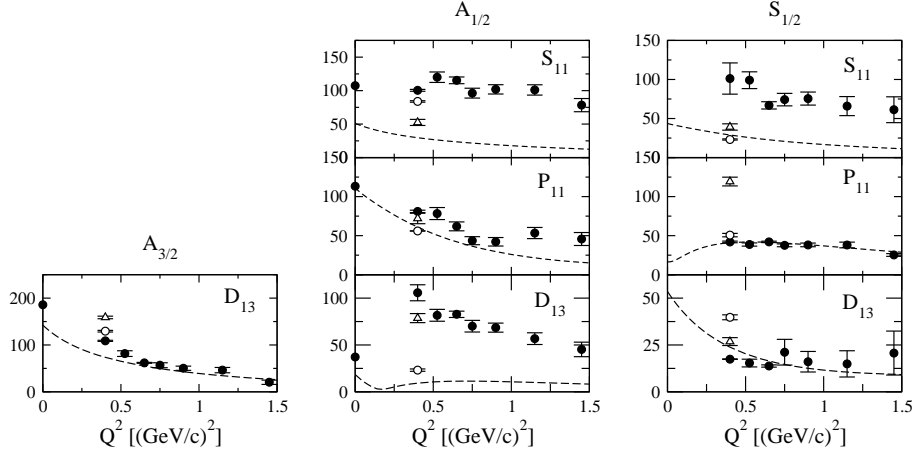


Fig. 2. Extracted helicity amplitudes for S_{11} at $W = 1535$ MeV (upper panels), P_{11} at $W = 1440$ MeV (middle panels), and D_{13} at $W = 1520$ MeV (lower panels). Solid points are from Fit1; dashed curves are the meson cloud contribution. Open circles and triangles at $Q^2 = 0.4$ (GeV/c) 2 are from Fit2 and Fit3, respectively.

ial for higher resonance states because the unstable $\pi\Delta, \rho N, \sigma N$ channels open, and thus the direct comparison of the helicity amplitudes from other analyses becomes unclear.

At $Q^2 = 0.4$ (GeV/c) 2 , the data of all structure functions both for $p(e, e'\pi^0)p$ and $p(e, e'\pi^+)n$ are available as seen in Table. 1. To see the sensitivity of the resulting helicity amplitudes to the amount of the data included in the fits, we further carry out two fits at this Q^2 , referred to as Fit2 and Fit3, respectively. Fit2 (Fit3) further includes the data of Refs. [11, 12, 13] (Ref. [11]) in the fit in addition to those of Ref. [10] which are used in Fit1. This means that Fit2 includes all available data both from $p(e, e'\pi^0)p$ and $p(e, e'\pi^+)n$, whereas Fit3 includes the same data but from $p(e, e'\pi^0)p$ only. The results of

each fit are the dashed and dotted curves in Fig. 1 for $p(e, e'\pi^0)p$ and Fig. 3 for $p(e, e'\pi^+)n$, respectively.

The corresponding change in the dressed helicity amplitudes are also shown as open circles and triangles in Fig. 2. A significant change among the three different fits is observed in most of the results. This indicates that fitting the data listed in Table 1 are far from sufficient to pin down the $\gamma^*N \rightarrow N^*$ transition form factors up to $Q^2 = 1.45$ (GeV/c) 2 . It clearly indicates the importance of obtaining data from complete or over-complete measurements of most, if not all, of the independent $p(e, e'\pi)N$ polarization observables. Such measurements were made by Kelly et al. [17] in the Δ (1232) region and will be performed at JLab for wide ranges of W and Q^2 in the next few years [1].

It has been seen in Fig. 3 that all of our current fits underestimate σ_T of $p(e, e'\pi^+)n$ at forward angles. We find that this can be improved by further varying the S_{31} and P_{13} bare helicity amplitudes within a reasonable range. We confirm that the same consequence is obtained also at other W , and find that the P_{13} (S_{31}) has contributions mainly at low (high) W . We also find that the inclusion of the bare S_{31} and P_{13} helicity amplitudes does not change other structure functions than σ_T of $p(e, e'\pi^+)n$ (the change is within the error). This indicates that those two helicity amplitudes are rather relevant to $p(e, e'\pi^+)n$, but not to $p(e, e'\pi^0)p$. As shown in Table 1, however, no enough data is currently available for $p(e, e'\pi^+)n$ above $Q^2 = 0.4$ (GeV/c) 2 . The data both of the $p(e, e'\pi^0)p$ and $p(e, e'\pi^+)n$ at same Q^2 values are desirable to pin down the Q^2 dependence of the S_{31} and P_{13} helicity amplitudes.

We now turn to show the coupled-channels effects (CCE). In Fig. 4, we see that when only the πN intermediate state is kept in the $M'B'$ summation of the non-resonant amplitude [Eq. (2)] and the dressed $\gamma^*N \rightarrow N^*$ vertices [Eq. (4)], the predicted total transverse and longitudinal cross sections σ_T and σ_L of $p(e, e'\pi^0)p$ are changed from the solid to dashed curves. This corresponds to only examining the CCE on the electromagnetic (Q^2 -dependent) part in the $\gamma^*N \rightarrow \pi N$ amplitude. All CCE on the non-electromagnetic interactions are kept in the calculations. We find that the CCE tends to decrease when Q^2 increases. This is rather clearly seen in σ_T . In particular, the CCE on σ_T at high $W \sim 1.5$ GeV is small (10-20%) already at $Q^2 = 0.4$ (GeV/c) 2 . (The effect is about 30-40% at $Q^2 = 0$.) This is understood as follows. In Eq. (3) we can further split the resonant amplitude t^R as $t^R = t_{\text{bare}}^R + t_{\text{m.c.}}^R$, where t_{bare}^R and

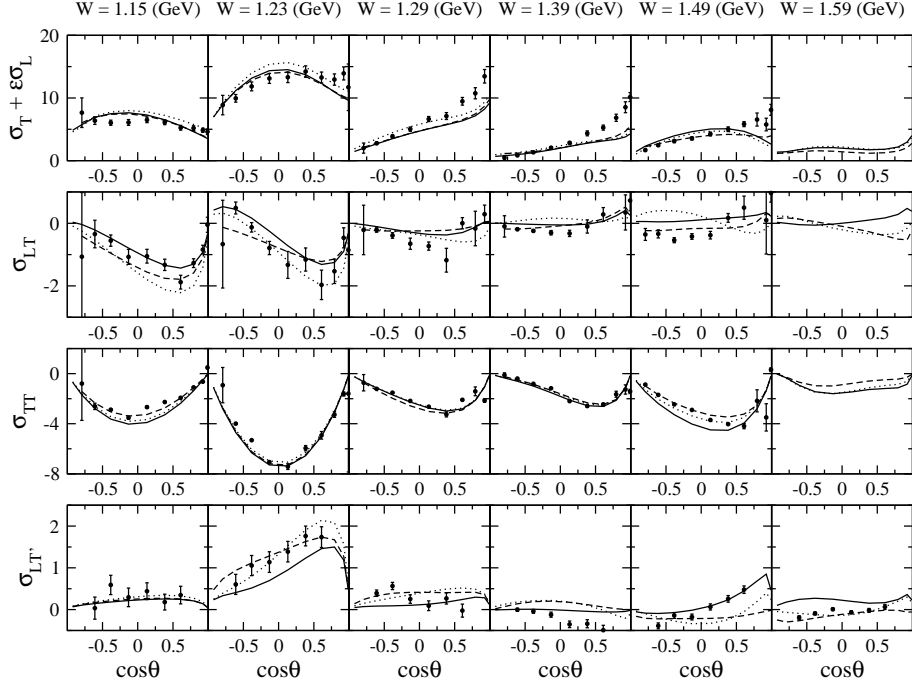


Fig. 3. Structure functions of $p(e, e' \pi^+)n$ at $Q^2 = 0.4$ (GeV/c) 2 . Here $\theta \equiv \theta_\pi^*$. The solid curves are the results of Fit1, the dashed curves are of Fit2, and the dotted curves are of Fit3. (See text for the description of each fit.) As for the $\sigma_{LT'}$, results at $W = 1.14, 1.22, 1.3, 1.38, 1.5, 1.58$ GeV (from left to right of the bottom row) are shown, in which the data are available. The data in the figure are taken from Ref. [12, 13].

$t_{m.c.}^R$ are the same as t^R but replacing $\bar{\Gamma}_{N^*, \lambda_\gamma \lambda_N}^J$ with its bare part $\Gamma_{N^*, \lambda_\gamma \lambda_N}^J$ and meson cloud part [the second term of Eq. (4)], respectively. The CCE shown in Fig. 4 comes from $t_{LSN\pi N, \lambda_\gamma \lambda_N}^J$ and $t_{m.c.}^R$. We have found that the relative importance of the CCE in each part remains the same for increasing Q^2 . However, the contribution of non-resonant mechanisms both on $t_{LSN\pi N, \lambda_\gamma \lambda_N}^J$ and $t_{m.c.}^R$ to the structure functions decreases for higher Q^2 compared with t_{bare}^R . This explains the smaller CCE compared with the photo-production reactions^[4]. The decreasing non-resonant interaction at higher Q^2 is due to its long range nature, thus indicating that higher Q^2 reactions provide a clearer probe of N^* . We obtain similar results also for $p(e, e' \pi^+)n$.

It is noted, however, that the above argument does not mean CCE is negligible in the full $\gamma^* N \rightarrow \pi N$ reaction process. In the above analysis we kept the CCE on the hadronic non-resonant amplitudes, the strong N^* vertices, and the N^* self-energy, which are Q^2 -independent and remain important irrespective of Q^2 . We have found in the previous analyses^[3, 6] that the CCE on them is significant in all energy region up to $W = 2$ GeV.

3 Summary and outlook

We have explored how the available $p(e, e' \pi)N$ data can be used to determine the $\gamma^* N \rightarrow N^*$ transition form factors within a dynamical coupled-channels model. Within the available data, the $\gamma^* N \rightarrow N^*$ bare helicity amplitudes of the first N^* states in S_{11} , P_{11} , P_{33} and D_{13} can be determined in the considered energy region, $W \leq 1.6$ GeV. We further observe that some of these parameters can not be determined well. The uncertainties could be due to the limitation that only data of 4 out of 11 independent $p(e, e' \pi)N$ observables are available for our analysis. The data from the forthcoming measurements of double and triple polarization observables at JLab will be highly desirable to make progress.

We found that the underestimation of the σ_T of $p(e, e' \pi^+)n$ at forward angles can be improved by further considering the S_{31} and P_{13} bare helicity amplitudes. Furthermore, these amplitudes can have relevant contribution to $p(e, e' \pi^+)n$, but not to $p(e, e' \pi^0)p$. The $p(e, e' \pi^+)n$ data of wide Q^2 region as well as $p(e, e' \pi^+)n$ seem necessary for determining the Q^2 dependence of the S_{31} and P_{13} helicity amplitudes.

For testing theoretical predictions from hadron structure calculations such as LQCD, the quantities of interest are the residues of the $\gamma^* N \rightarrow \pi N$ ampli-

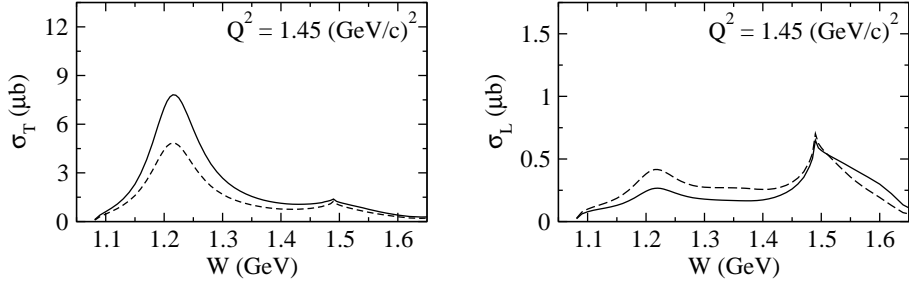


Fig. 4. Coupled-channels effect on the integrated structure functions $\sigma_T(W)$ and $\sigma_L(W)$ for $Q^2 = 1.45$ $(\text{GeV}/c)^2$ for $p(e, e'\pi^0)p$ reactions. The solid curves are the full results calculated with the bare helicity amplitudes of Fit1. The dashed curves are the same as solid curves but only the πN loop is taken in the $M'B'$ summation in Eqs. (2) and (4).

tudes, defined by Eqs. (1)-(4), at the corresponding resonance poles. If the resonance poles are associated with the amplitude $t_{LS_N\pi N, \lambda_\gamma \lambda_N}^{R,J}(k, q, W, Q^2)$ of Eq. (3), the extracted residues are directly related to the dressed form factors $\bar{\Gamma}_{N^*, L'S'M'B'}^J(k', W)$. An analytic continuation method for extracting these information has been developed ^[18], and our results along with other hadronic properties associated to nucleon resonances will be published elsewhere. Let us mention that the extracted form factors are complex numbers and some investigations are needed to see how they can be compared to the usual helicity amplitudes, which are real numbers, listed by PDG ^[19].

The author thanks H. Kamano, T.-S. H. Lee, A. Matsuyama and T. Sato, for the nice EBAC collaboration. This work is supported by a CPAN Consolider INGENIO CSD 2007-0042 contract and Grants No. FIS2008-1661 (Spain), by the U.S. Department of Energy, Office of Nuclear Physics Division, under contract No. DE-AC02-06CH11357, and Contract No. DE-AC05-06OR23177 under which Jefferson Science Associates operates Jefferson Lab. This work used resources of the National Energy Research Scientific Computing Center which is supported by the Office of Science of the U.S. Department of Energy under Contract No. DE-AC02-05CH11231.

References

- 1 V. Burkert and T.-S. H. Lee, Int. J. of Mod. Phys. **E13**, 1035 (2004).
- 2 A. Matsuyama, T. Sato, and T.-S. H. Lee, Phys. Rep. **439**, 193 (2007).
- 3 B. Julia-Diaz, T.-S. H. Lee, A. Matsuyama, and T. Sato, Phys. Rev. C **76**, 065201 (2007).
- 4 B. Julia-Diaz, T.-S. H. Lee, A. Matsuyama, T. Sato, and L. C. Smith, Phys. Rev. C **77**, 045205 (2008).
- 5 J. Durand, B. Julia-Diaz, T.-S. H. Lee, B. Saghai, and T. Sato, Phys. Rev. C **78**, 025204 (2008).
- 6 H. Kamano, B. Julia-Diaz, T.-S. H. Lee, A. Matsuyama, and T. Sato, Phys. Rev. C **79**, 025206 (2009).
- 7 B. Julia-Diaz, T.-S. H. Lee, T. Sato, and L. C. Smith, Phys. Rev. C **75**, 015205 (2007).
- 8 T. Sato and T.-S. H. Lee, Phys. Rev. C **54**, 2660 (1996).
- 9 T. Sato and T.-S. H. Lee, arXiv:0902.3653 [nucl-th].
- 10 K. Joo *et al.*, Phys. Rev. Lett. **88**, 122001 (2002).
- 11 K. Joo *et al.*, Phys. Rev. C **68**, 032201 (2003).
- 12 H. Egiyan *et al.*, Phys. Rev. C **73**, 025204 (2006).
- 13 K. Joo *et al.*, Phys. Rev. C **72**, 058202 (2005).
- 14 CLAS Physics Database, JLab (Hall B), <http://clasweb.jlab.org/cgi-bin/clasdb/db.cgi>.
- 15 T. Sato and T.-S. H. Lee, Phys. Rev. C **63**, 055201 (2001).
- 16 I. G. Aznauryan, V. D. Burkert, and T.-S. H. Lee, arXiv:0810.0997v2 [nucl-th].
- 17 J. Kelly *et al.*, Phys. Rev. Lett. **95**, 102001 (2005).
- 18 N. Suzuki, T. Sato, and T.-S. H. Lee, Phys. Rev. C **79**, 025205 (2009).
- 19 C. Amsler *et al.*, Phys. Lett. **B667**, 1 (2008).